Atmos. Meas. Tech. Discuss., 8, 9785–9821, 2015
www.atmos-meas-tech-discuss.net/8/9785/2015/
doi:10.5194/amtd-8-9785-2015

Atmospheric Measurement Techniques Discussions
Open Access

Inter-comparison of IASI and AATSR over an extended period

M. Bali[1], J. Mittaz[2], E. Maturi[3], and M. Goldberg[3]

[1]ESSIC/CICS, University of Maryland, College Park, MD, USA
[2]Department of Meteorology, University of Reading, Reading, UK
[3]National Oceanic and Atmospheric Administration, College Park, MD, USA

Received: 21 July 2015 – Accepted: 18 August 2015 – Published: 18 September 2015

Correspondence to: M. Bali (manik.bali@noaa.gov)

Published by Copernicus Publications on behalf of the European Geosciences Union.

Abstract

The launch of ENVISAT in 2002 and the launch of MetTop-A in 2006 put two highly accurate instruments in space to measure Top of Atmosphere (TOA) radiances. These instruments are the AATSR and IASI. While the AATSR, by design is a climate accurate (i.e. accuracy within 0.1 K and stability within 0.05 K dec^{-1}) instrument, the IASI is a hyperspectral instrument that has a stated accuracy of within 0.5 K. This accuracy and stability are used in producing climate CDR's from these instruments and also aids in using these instruments as benchmarks for inter-comparison studies that aim at measuring stability and accuracy of instruments that are concurrently flying with them. The GSICS (Global Space Based Inter-Calibration System) has extensively exploited the IASI by comparing its measurements with Polar as well as Geostationary satellite instruments and measuring the in-orbit stability and accuracy of these instruments. More recent re-calibration efforts, such as the NOAA CDR project that is aimed at recalibrating the AVHRR uses the IASI and the AATSR as references. However to trust the recalibrated radiances it is vital that the in-orbit accuracy of the reference sources is known and critical issues such as scan angle dependence, and temporal variation of the accuracy are fully evaluated across a large temperature range (200–300 K).

In order to better understand the accuracy and asses the trustworthiness of these references we present here a comprehensive analysis of the AATSR–IASI bias derived from their collocated pixels, over the period January 2008 through March 2011. Our analysis indicates that generally the AATSR (Nadir View) and IASI can act as good reference instruments and IASI is much more accurate than its design specification. In fact, taking into account a small bias the AATSR–IASI bias is close to the AATSR pre-launch bias implying that IASI can get close to pre-launch levels of accuracy. We also examine temperature dependent bias in the AATSR at low (< 240 K) temperatures which seems to appear after orbit was lowered of the ENVISAT satellite and its inclination control was discontinued. In addition, a very small scan angular dependence of AATSR–IASI bias indicates that the AVHRR has a scan angle dependent bias.

AMTD
8, 9785–9821, 2015

We also examine the bias problem with the 12 µm channel of the AATSR in detail. We show that this bias not only has a temperature dependence (it grows up to 0.4 K at low temperatures) but also has a seasonal dependence in the SST (265–300 K) temperature range and is highly correlated to instrument temperature in the cold temperature range. We then discuss a possible method to correct the 11 and the 12 µm bias so as to use the corrected radiances for re-calibration of AVHRR.

1 Introduction

The Top of Atmosphere radiance (TOA) is a critical variable measured by satellites. Long time series of TOA (30 yr) are key input used in producing climate data records of Essential Climate Variables, and modern weather forecasting systems directly assimilate TOA radiances in order to produce forecasts. Hence there is a critical need to accurately measure the TOA radiances for long period of time (at least 30 yr, Leroy et al., 2008) so that climate signals can be extracted from these measurements. In fact it is suggested (Ohring et al., 2005) that the TOA measurement accuracy should be better than 0.1 K and its stability better than 0.05 K dec^{-1}.

Achieving such stringent accuracy and stability requirement is a challenge. Despite the fact that modern instruments undergo advanced pre-launch calibration procedures and are sometimes equipped with SI traceable black bodies (e.g. the Advanced/Along Track Radiometers A/ATSR series), once the instrument reaches the space environment its characteristics can change and TOA measurement can develop systematic or random biases. Therefore in order to maintain climate constraints in TOA measurements, it is essential to first keep track of in-orbit biases and subsequently employ corrective measures whenever necessary.

In recent years, inter-comparison of TOA measurements between concurrently flying satellites has evolved as a dependable method to measure in-orbit TOA biases on the fly. Entities such as Global Space Based Inter-Calibration System (GSICS) routinely use (Infrared Atmospheric Sounding Interferometer) IASI as a “reference source”

AMTD
8, 9785–9821, 2015

to validate TOA measurements taken by other satellites (such as AIRS, GOES and MSG), and diagnose and correct any biases (Wang et al., 2010; Yu et al., 2012). Even outside the GSICS community IASI is widely used as a reference source. For example, a comparison of AVHRR and IASI radiances detected several issues with AVHRR measurements of TOA including temperature and scan angle dependent biases in the AVHRR TOA measurements (e.g. Wang and Cao, 2008). Mittaz and Harris (2011) subsequently developed a new calibration scheme by developing a physical model of the AVHRR instrument that uses IASI as a "reference source" and this new calibration scheme brought TOA measurements close to thresholds of climate readiness.

In the case of AVHRR this cycle of TOA inter-comparison with a reference source, detecting biases and then subsequently correcting them by developing a new calibration scheme has far reaching implications for data used for climate research. This is because the AVHRR has approximately 35 yr of TOA measurements which makes it one of the few sensors which cover enough time to be legitimately used for climate studies. If by using the new calibration scheme, the accuracy of this time series can be bought to near climate ready levels it can become a good candidate for climate research.

However, in this calibration scheme the choice of TOA reference sources plays a central role. IASI, though widely used, has a short history and can act as a reference only from 2006 onwards whereas the AVHRR series dates back to 1979. AIRS (Atmospheric Infrared Sounder, another commonly used hyperspectral sounding instrument) only dates back to 2000. Prior to that, the only credible TOA reference is the Advanced Along Track Radiometer series of "climate satellites" (ATSR-1 launched in 1991, ATSR-2 in 1995 and the AATSR in 2002). Given that, to produce climate data records we cannot use a single reference this brings us to the obvious question whether these references (i.e. A/ATSR and IASI) are stable and accurate enough (i.e. climate ready) to be used as accurate TOA reference sources.

A previous study by Illingsworth et al., 2009 used the AATSR as a benchmark and attempted to measure the bias in IASI vs. AATSR. Using a small number of colloca-

AMTD
8, 9785–9821, 2015

tions (41 for clear sky and 66 for homogenous scenes) taken from a single orbit of 1 September 2007 over oceans, this study concluded that the mean 11 and 12 µm IASI and AATSR measurements agree to within −0.05 and 0.23 K respectively in the SST range.

This study succeeded in getting to what was sufficient for a basic estimate of differences between IASI and the AATSR. However, the small size was insufficient for answering key questions about the possible variations of bias with scan angle, scene temperature and time which still need to be addressed in order to form an opinion about the climate readiness of these instruments and their use for recalibration studies. In terms of the AATSR there are additional possible issues such as the known BT offset of order −0.2 K in the 12 µm channel when compared to the ATSR-2 (Corlett, 2014; Smith, 2007). This offset is most likely a calibration issue that occurred post launch and possible causes range from change in detector characteristics to changes in the (Spectral Response Function)SRF characteristics (position and shape). An intercomparison of AATSR with the IASI gives a unique opportunity to directly test different theories regarding the origin of this bias.

The goal of this paper is to measure the trustworthiness of the AATSR and IASI for use in re-calibration by revealing the full extent of the AATSR–IASI measurement bias over a wide range of scan angles, temperature (210–310 K) and time (2008–2010 plus three months of 2011). We also suggest a method that utilizes AIRS as a transfer between IASI and ATSR2 (another AATSR family instrument) to assess the spectral dependence of the IASI bias (i.e. weather bias in 11 and 12 µm spectral bands of the IASI stays same or can be channel dependent) and then correct for post launch temperature dependent measurement bias anomalies such as seen in the AATSR 12 µm channel. In the next two sections we give a brief description of the AATSR and the IASI instruments and then in the following section we describe our inter-comparison method. The results section first addresses the issue of scan angle dependence of the AATSR–IASI bias. Subsequently the temperature and time dependence of the AATSR–IASI bias is presented in addition to the impact of SRF shift on the temperature dependent bias

AMTD
8, 9785–9821, 2015

of the 12 µm channel. The impact of change in orbital parameters on using AATSR as a credible reference source is also evaluated.

2 Instrument description and collocation algorithm

2.1 Advanced Along Track Scanning Radiometer (AATSR)

The Advanced Along Track Scanning Radiometer (AATSR) belongs to the family of ATSRs (ATSR-1, ATSR-2 and AATSR) and was designed to be a climate ready instrument (Llewellyn-Jones et al., 2001). From its launch (onboard ENVISAT) in 2002 until May 2012 it had observed the earth in four visible (0.555, 0.659, 0.865 and 1.61 µm) and three IR bands (3.7, 11 and 12 µm) and has provided continuity to the earlier launches of ATSRs (launched in 1991 and 1995).

In order to achieve an accuracy of the scale of climate readiness the AATSR uses a highly sophisticated calibration mechanism (Llewellyn-Jones et al., 2001; Smith et al., 2001, 2012). This calibration mechanism uses two SI traceable black bodies that are situated at either edge of the SST temperature range (approximately 263 and 301 K) which are used as calibration references. Since these references are at either edge of the SST range the effect of detector nonlinearity within the SST range gets pinned down. This reduces possible calibration errors while as it maintaining high intrinsic sensitivity (Smith et al., 2001, 2012). The detectors themselves are maintained at a constant temperature of 80 K which ensures stability and keeps the radiometric noise at 270 K to within 0.05 K.

The AATSR has a conical scan and views a location at two zenith angles. It produces two swaths (500 km each) at nadir and forward view with a spatial resolution of 1 km × 1 km at nadir and 1.5 km × 2.0 km at the forward view. Locations of the forward view are viewed again at nadir as the satellite moves forward. For the purpose of intercomparison we have used the AATSR Level 1B gridded data sets. This data is the

AMTD
8, 9785–9821, 2015

observed TOA radiance that is geo-located and re-sampled to 1 km × 1 km resolution everywhere (every pixel of forward as well as nadir views).

The two IR channels (11 and 12 µm) of the AATSR overlap the IR spectrum of IASI. Since the ENVISAT flew concurrently with METOP-A it can act as a credible reference to validate the measurements taken by IASI.

2.2 Infrared Atmospheric Sounding Interferometer (IASI)

The IASI is a hyper spectral instrument that observes the earth in IR bands (Phulpin et al.,2007; Clerbaux et al., 2007). It is recognized by the GSICS as a benchmark for inter- satellite comparison of TOA (e.g. Wu et al., 2009). It works on the principal of a Michelson's interferometer and was launched onboard Metop-A in 2006. It consists of a Fourier Transform Spectrometer with an imaging system which provides infrared spectra between 645 and 2760 cm^{-1} (3.6 to 15.5 µm) at a resolution of 0.25 µm (EUMETSAT 2012). The IASI takes these observations in a step and stare mode and covers the ±47.85° range in 30 steps in every 8.0 s scan cycle, with 3.3° for each step (normal mode). IASI has a pixel resolution of 12 km at nadir with four pixels per view each positioned in the cross- and along-track directions located at ±0.825° from the center point. The measured inter-ferograms are processed by an onboard digital processing subsystem to reduce the data transmission rate. This subsystem also performs the radiometric calibration (based on the measurements of cold and warm reference targets, i.e., deep space and an onboard blackbody), and nonlinearity corrections. Ground system processing takes over once this data are received at the ground. The main components of the ground processing are radiometric post calibration, spectral calibration, and apodization. The main output of this ground processing is a resampled, apodized, and calibrated spectrum with 8461 spectral samples and that product is known as the IASI level-1C radiance product and is used for our inter-comparison.

AMTD
8, 9785–9821, 2015

2.3 Collocation method

The collocation method is a critical part of any satellite inter-comparison study. Its purpose is to identify pixel pairs (one from each sensor) when a given target is simultaneously viewed by two sensors at nearly the same time under similar viewing conditions thus enabling a direct comparison of likes with likes. Accuracy and selection criteria of pixel pairs that are finally considered for comparison are fundamental parameters of a collocation algorithm. The latter has been discussed by Wu et al. (2009), wherein GSICS provided a baseline criterion for pixel pair selection during inter-comparison. Within the error bounds of geolocation errors, application of this criterion results in selection of scenes that are uniform, viewed with similar viewing angle around the same time. Thresholds for viewing angle and observation time differences are stated in Table 1. Selection of uniform scenes ensures that the effects of geolocation errors and effects of differing spatial resolution of the pixel pairs is minimized when their radiances are compared.

For the AATSR and IASI inter-comparison, a new collocation algorithm was developed that inherited some of the selection criteria from the GSICS baseline. This algorithm took the IASI (Level-1C) granules and AATSR (gridded Level-1B) orbital files as input and identified AATSR pixels of nadir and forward view that were collocated within the larger IASI pixel. In order to achieve a high degree of accuracy, the exact shape and size of the IASI pixel as it varied with scan angle was computed using standard trigonometric functions and used for the collocation. To ensure correctness of the algorithm underwent strict unit testing. A test bed was created which used two scenarios. First the algorithm was given AATSR scene compared against the same AATSR scene and the algorithm was run to ensure that all the AATSR pixels were collocated with themselves. The second test used simulated scenes in which the expected number of collocations in the larger pixel was already known. The collocation algorithm was used only when it passed both these tests.

AMTD
8, 9785–9821, 2015

This tested algorithm was used to identify AATSR IASI collocated pixels from January 2008–March 2011. For a given IASI AATSR collocation, the IASI footprint on the ground is larger (12 km at nadir) than the AATSR (which is re-sampled to make it 1 km everywhere on the swath) so several AATSR pixels fall within each IASI pixel. In order to ensure scene uniformity within the IASI footprint, thresholds are set regarding the standard deviation (SD) of the AATSR pixels within the IASI footprint (Table 1). However setting this threshold alone does not guarantee that the state of the scene viewed by the two instruments remains homogenous and invariant during the time it is viewed by the two satellites. It is possible that clouds move into the IASI pixel within the threshold time (time between two satellite viewings of the same target) and break the homogeneity after the test is applied. To ensure that such IASI pixels are identified and subsequently rejected, a second SD threshold test is also applied. For this a perimeter area of 5 AATSR pixels around an IASI pixel (Fig. 1) is selected and SD is computed for this set of AATSR pixels. Only those IASI pixels that for which even the SD of perimeter pixels is less than 1 were selected for further comparison. In the end the IASI spectrum for these collocations is integrated over the AATSR SRF (Eq. 1) to get IASI representative radiances. In this integration all the IASI radiances that fall within the range of (9.82–12.18 µm) were used to get 11 µm IASI representative radiances and all the IASI (real not pseudo channels) radiances in the range (11.02–13.40) µm to get the 12 µm IASI representative radiances. These wavelength ranges have been taken form the AATSR stated SRF ranges. These radiances are then compared with the mean radiances of the AATSR that are collocated with the IASI pixel.

$$\text{IASI Rep Rad} = \frac{\sum \text{IASI\_RAD} \times \text{SRFVAL}}{\sum \text{SRFVAL}} \quad (1)$$

AMTD
8, 9785–9821, 2015

3 Collocation results

3.1 Scan angle dependence of bias

Many modern earth observation instruments are known to show measurements bias with respect to scan angle, and this problem has been observed in instruments observing in variety of bands. For example GOME (UV bands), AMSU (microwave bands), AVHRR (IR bands) (Snel, 2001; Tanzi, 2001; Wu, 2004; Wang and Cao, 2008; Mittaz and Harris, 2011) have scan angle dependencies in TOA measurements to varying degrees. The reasons for scan angle dependence are not absolutely clear but it is hypothesized that it is due to the variation in polarization (Wang and Cao, 2008) that occurs when incident radiant flux originating from the target scene falls on the scan mirror at different angles while it is scanning (rotating). Since the root cause of this dependence is not fully understood, and so far has not been physically modeled, this dependence usually does not go away by employing a better calibration technique. Modern instruments such as the AATSR and IASI are known to apply empirical algorithms (such as response vs. scan angle correction) that aim to correct this dependence, however the effectiveness of these algorithms is not fully known.

In the case of AVHRR this problem was identified when AVHRR vs. IASI (onboard Metop-B) inter-comparisons were made. Further AVHRR vs. IASI comparisons (Mittaz and Harris, 2011)showed that this scan angle dependent bias was also temperature dependent and it attained a maximum (~ 1.2 K at 40° zenith angle) over low temperature (200–220 K) at limb view. Over the SST temperature range, this study showed no scan angle dependent bias. However, from this AVHRR IASI comparison it was not clear whether the scan angle dependent bias at low temperature was an IASI effect or an AVHRR effect. From the recalibration point of view it was important to see if the reference instruments (AATSR and IASI) had any scan angle dependence and if they do then quantify its magnitude. The 12 µm channel of AATSR has a known offset of 0.2 K. As would be seen later, it has complex temperature and time dependence so it is not used to measure the scan angle dependence.

AMTD
8, 9785–9821, 2015

Figure 2 shows the variation of AATSR IASI 11 µm bias over the entire range of the IASI and AATSR scan angle in cold and SST temperature ranges. While the bias between −20 to 20° comes from the collocations between the nadir view of AATSR and the IASI, the biases beyond ±40° IASI scan angle come from collocations between the forward view of AATSR and the IASI. Both these views show different characteristics. The AATSR vs. IASI bias at nadir view is nearly constant with some residual errors ($\sim 0.0025\,\mathrm{K\,deg^{-1}}$ of satellite zenith angle) and a constant offset of nearly zero. Given the fact that the scan angle dependent variation of the bias at the nadir view is very small, the scan angle dependent bias between AVHRR and IASI seen by Mittaz and Harris was a AVHRR effect and not a IASI effect.

The bias between the AATSR forward view and the IASI seem to show a scan angle dependence in both temperature ranges (cold ∼ 0.7 K and SST ∼ 0.3 K). Two important parameters need to be considered while analyzing this bias 1). The two instruments look at the same target pixel but they look through different atmospheres. The AATSR forward views are measurements taken along track while the IASI measurements are taken on targets across its motion track. This can result in differing measurements of TOA radiance by the two instruments. 2). The AATSR forward view has known geolocation errors. These errors magnify at the poles.

Corlett (2008) noted alignment issues with the AATSR forward view wherein the forward-view minus nadir-view image shows significant edge effects around the eddy structures and also at the edges of clouds. Such alignment issues lead to geolocation errors in the forward view particularly at cloud edges which are characterized by low temperature. From the point of view of recalibration bias computed from the AATSR, only the nadir view is used as a reference.

AMTD
8, 9785–9821, 2015

3.2 Temperature dependence of the AATSR-IASI bias

3.2.1 11 µm

Figure 3 shows the variation of AATSR–IASI bias over a temperature range of 200–300 K. The temperature range chosen here (210–300 K) is similar to the one used by Smith et al. (2012) to depict the difference between the temperature measured by the AATSR and that of a black body that it observed during pre-launch testing. During pre-launch testing the accuracy of the AATSR instrument was quantified by calculating the difference between the target temperature and AATSR instrument measured temperature from an ensemble of measurements wherein the viewing target's (a blackbody) temperature was varied from 200–320 K at intervals of 5 K. This temperature range also includes the range (275–300 K) used by Illingworth et al. (2009) to study the AATSR–IASI difference. Hence our choice of this range gives us the opportunity to compare and verify our inter-comparison results with two independent studies, one done at pre-launch and another carried out post-launch but with limited sample size.

The mean bias of the AATSR–IASI difference over the entire temperature range is of the order of −0.075 K (±0.03 K). However the AATSR–IASI bias variation in the 210–300 K range is similar to the difference that was observed by Smith et al. (2012), during the pre-launch testing. The characteristic dip at the low temperature (< 230 K) and the hump at 245 K are captured well. If one applies a offset of −0.130 K to the AATSR–IASI variation curve, the pre-launch and the post launch (i.e. our inter-comparison) variations match to within a few hundredth of a degree K. The maximum difference between the AATSR pre and the post launch is 0.04 K at 280 K and at all other temperatures both curves match better than this. The −0.11 K offset has been computed by minimizing the root mean square difference between the post and the pre-launch curves.

Since the AATSR pre-launch calibration has a known negative bias of the order of 0.0–0.05 K referenced to SI calibrated sources, and the inter-comparison of AATSR–IASI inter-comparisons show a positive bias of the order of 0.07 K (Fig. 3), the observed

AMTD
8, 9785–9821, 2015

positive AATSR–IASI bias is likely to be an IASI bias relative to the AATSR. Since in the SST temperature regime the AATSR is thought to be absolutely accurate to a few hundredths of a degree, the implication is that IASI (when corrected for this small bias) can generate radiances that are almost as accurate as prelaunch data to within a few hundredths of a degree.

Our inter-comparision results also agree with the AATSR–IASI comparisions of Illingworth et al. (2009) to a level of a a few hundreth of degree. While our mean difference over the entire temperature range is −0.075 K (±0.03 K), Illingworth et al. difference is of the order of 0.05 K (±0.03 K). The small difference between the two comparisons can be attributed to the difference in data sets.

3.2.2 12 µm

Immediately after the launch of the AATSR onboard ENVISAT it was found that the 12 µm channel had an apparent BT offset of ∼ −0.2 K in the SST temperature range when compared with the ATSR-2 (Corlett, 2014). It was verified by Smith (2007) to be an AATSR artifact.

However, our analysis has shown that the BT offset is strongly temperature dependent and steadily grows to about 0.4 K as the temperatures decreases to 200 K (Fig. 4). At SST temperatures the bias is negative and taking into account the small (0.07 K) IASI bias discussed above is approximately consistent with the previously known bias of −0.2 K. Among the possible reasons of this effect is that the SRF may have undergone a shift or a possible long wave leak developed post launch (Smith, 2007).

We have investigated the possibility of a simple SRF shift explaining the bias by undertaking two sets of experiments. In the first set the SRF was shifted by $+n$ wave numbers (where $n = 1,2,3,4,5,6$). The second set of experiments the SRF was shifted by –n wave numbers (where $n = -1,-2,-3,-4,-5,-6$). Figure 5 shows the impact of shifting the SRF on the AATSR–IASI bias for each "$+n$". As shown in Fig. 5, the temperature dependence of the bias is preserved right up until a shift of +6 wave number is

AMTD
8, 9785–9821, 2015

applied. A similar conclusion was drawn with the $-n$ shifts (not shown) and the overall conclusion is that SRF shift is an unlikely solution to the temperature dependent bias.

While further investigation into possible causes of the bias is beyond the scope of this study we have derived a simple correction scheme that can be used in recalibration studies. Even though the 12 µm channel bias is large it is very stable so it is possible to empirically correct these radiances by fitting a polynomial.

3.3 Temporal dependence of IASI bias

Legacy instruments such as the AVHRR are known to show seasonal variation in radiance measurements. This variation is mainly attributed to seasonal variation in instrument temperature. Mittaz and Harris (2011) have shown that this seasonal effect can be removed by using a better calibration scheme that physically models the effects of seasonal changes in instrument temperature. However, this scheme needs stable references that are minimally impacted by instrument temperature. Since IASI and AATSR are envisaged to be used as references in the AVHRR re-calibration, it is vital to understand and quantify the seasonal variation in the measurement.

Figure 6 shows the AATSR–IASI bias variation with respect to time in two temperature ranges (< 230 and > 240 K) for the period January 2008–March 2011. The AATSR–IASI bias in these two temperature ranges display different behaviors.

3.3.1 Warm temperature range (Temp > 230 K)

The temperature of the two calibration blackbodies in the AATSR instrument lie in this warm temperature range (260 K cold and 310 K warm). This helps in pinning down the effect of detector nonlinearly and ward off effects of seasonal changes in instrument temperature. The robustness of this calibration system is clearly demonstrated when month-to-month AATSR–IASI bias was analyzed. As seen in Fig. 6 the 11 µm channel maintains a very well-calibrated stance with small annual deviations (±0.01 K) around its mean value of 0.078 K (Fig. 6).

AMTD
8, 9785–9821, 2015

The 12 µm channel of AATSR–IASI bias shows slightly larger amplitude (0.042 ± 0.032 K) than the 11 µm channel, in this temperature range. Despite the known temperature dependent BT offset (Fig. 6) of this channel, the calibration mechanism ensures that the seasonal variability in the AATSR–IASI bias at the warm temperature range remains confined to less than a few hundredths of a degree K. So the seasonal variation in the warm temperature range in both the channels can be stated as very small (a few hundredths of degree).

3.3.2 Cold temperature range (Temp < 230 K)

The cold temperature range lies outside the temperature range spanned by the two calibration blackbodies of the AATSR. Since the method of correcting for the detector nonlinearity is not perfect the AATSR pre-launch data (Fig. 3) show a slightly larger bias in this range. A similar characteristic is displayed post launch when AATSR is compared with IASI over several months. This inter-comparison shows that the 11 µm channel (Fig. 6) bias is slightly higher than that seen at the warm temperature range and hovers around 0.086 K (±0.022 K).

A similar analysis of the 12 µm channel AATSR–IASI bias reveals a larger seasonal variation of 0.31 K (±0.03 K) as compared to the 11 µm. Within a given year there are two distinct peaks. For this channel, the entire AATSR–IASI bias curve is closely cross correlated (Fig. 6) with the base plate temperature variation (cross correlation = 0.78) thereby indicating that the instrument temperature could be influencing the AATSR measurements in this temperature range for this channel.

In the 11 µm channel, some months (November and December), show temporary spikes of the order of 0.15 K that stands out. Since these spikes occur during the time of "year end orbit maneuver of ENVISAT" (Noll, 2010) it is likely that these are caused by temporary geo-location errors and not calibration errors of the AATSR or the IASI. For 2008 and 2009 these spikes are nearly same; the spike in end of 2010 appears unique as it is followed by an anomalous dip in January 2011.

AMTD
8, 9785–9821, 2015

It must also be noted that the orbit maneuver carried out in October 2010 was different from the ones carried out in prior years because orbital inclination control was switched off and the altitude of the satellite was reduced by 17.4 Km (Miranda et al., 2010). This led to a new 30 day repeat cycle (431 orbits per cycle), instead of the earlier 35 day repeat cycle (501 orbits per cycle). It was envisaged that this would not cause any anomalies in AATSR measurements and initial testing immediately after the maneuver did not detect any anomaly (Cocevar et al., 2011).

However it must be noted that changes in orbital inclination are slow and their impacts would not be visible in the first few orbits that were used in the testing phase (Cocevar, 2013) and can be detectable only in the subsequent months. By extending the inter-comparison several months beyond October 2010 (i.e. until March 2011) our inter-comparison study was able to detected the impact of this maneuver on AATSR measurements as a spike that starts in November 2010 and lasts till February 2011.

Since such spikes can impact the AVHRR recalibrating process, we investigated the full scale of these spikes. Figure 7 shows the temperature dependence of AATSR–IASI bias for the DJF for the 11 and 12 µm channels. This figure shows that while the 2008 and 2009 spikes show small deviations at the cold temperature end the bias for 2010–2011 shows a clear temperature dependent trend.

This trend in 2011 is important as it can impact the re-calibration of the AVHRR from 2011 onwards if AATSR is to be used as a reference for this period. Further analysis (Fig. 8) showed that this trend is confined to collocations between the AATSR and IASI over Greenland. Figure 9 shows the biases for the same months (DJF) when Greenland is excluded and one can see that the trend is removed.

Given that AATSR's onboard calibration has worked well prior to this maneuver and has even replicated pre-launch behavior for months prior to October 2010, the trend seen here does not appear to be a calibration issue as change in orbital parameters would not be able to influence the robust onboard calibration scheme. However it appears that changes in satellite altitude and without a check on inclination control can lead to geolocation errors that can lead to trends at higher latitudes.

AMTD
8, 9785–9821, 2015

It must be noted that a similar trend is not found in the diametrically opposite position in the Southern Hemisphere where the SNO between AATSR and IASI also overlap under similar conditions as they do over Greenland. All the collocations between −60–82° S occur over ocean. Since spatial temperature gradients over the oceans are not as sharp as those over land (i.e. neighboring pixels have nearly the same temperature value), any offsets in those pixel location due to errors in geo-location would not show up as a temperature bias. So the higher latitudes of the Southern Hemisphere are not good target areas for detecting geo-location errors.

3.4 Other dependencies of AATSR IASI bias

During the course of this study, dependence of the AATSR–IASI bias on day/night and land/sea scenes was investigated. While it was noted that there is a significant rejection (due to application of thresholds stated in Table 1) of pixels over land as compared to scenes selected over sea, but such rejection only influenced random noise associated with the AATSR–IASI bias. Similar results were found when day scenes were compared with night scenes. In this comparison the number of pixels passing the thresholds was not impacted and the bias remained unchanged. This demonstrated the robustness of the onboard calibration of the two instruments.

3.5 A correction for the AATSR 11 and 12 µm Channel

Another key goal of the AATSR IASI inter-comparisons is to make available the most accurate and trusted radiances as references to the AVHRR re-calibration process. Smith et al. (2012) indicate that the AATSR instrument had a small temperature dependent bias in the 11 and 12 µm channels (∼ −0.05 K at SST range and ∼ −0.1 at 200–230 K) when compared with trusted SI traceable targets at pre-launch. For the AVHRR re-calibration we need the radiance of the trusted SI traceable target. At pre-launch one can get this radiance if one applies a correction to the AATSR measured radiances. In this case the correction would be the polynomial fit to the AATSR 'SI trace-

AMTD
8, 9785–9821, 2015

able reference target difference (vs. SI radiance). We call the radiance of this trusted SI traceable target as the "True Value".

Normally the pre-launch environment is not replicated post launch. Despite the stated accuracy of IASI (~ 0.5 K; Blumstein et al., 2002) its wavelength, time and temperature dependent offsets and biases in the space environment are not completely known. A first estimate of the IASI offset is shown in Fig. 3 which shows that for the 11 µm channel the IASI is nearly (to a 100th of K) as good as a pre-launch reference (with an offset). This means that after applying sufficient corrections and offsets, the IASI in principle can come close to the trusted radiances of SI-traceable targets; i.e. the "True Value". These corrections and offsets that need to be applied to the IASI can be determined when IASI is compared to a third reference instrument that is similar in accuracy and stability as the AATSR.

The ATSR-2 onboard ERS-2 is a good candidate that can act as a third reference. This is because it is the predecessor of AATSR and is similar to it (dual view, two black bodies, and by design climate-accurate) but it stopped functioning in April 2003 well before IASI was launched. Since AIRS is a hyperspectral instrument that has overlapping time window both with ATSR-2 and IASI, it can be used as a transfer to determine IASI offsets with ATSR-2. In addition, AIRS has been extensively compared with IASI.

In-orbit, we employ a two step process to calculate the True Value. First we determine the IASI radiances from the AATSR radiance by using the AATSR–IASI difference curve. Then we apply a correction (offset) to this IASI radiance. This correction (offset) is calculated by taking into account the IASI offset with AIRS and subsequently ATSR-2.

A recent inter-comparison between AIRS and IASI by Wang et al. (2010 and 2011) attempted to compare IASI with AIRS by two methods, by direct SNO method and by using GOES-11 as a transfer. Since both the instruments have different equator crossing times, most of the SNO collocated pixels are located near the poles and in essence are mainly confined to low temperature range (200–230 K). On the other hand

AMTD
8, 9785–9821, 2015

when GOES-11 is used as a transfer collocated pixels are confined to SST temperature range. Table 2 shows a summary of the results.

Complimentary to Wang's analysis we have created 3 month inter-comparisons of AIRS with ATSR2 (September 2002–November 2002). These are shown in Fig. 9 below.

This figure shows that for most part, AIRS is nearly as good a reference as the pre-launch reference for the ATSR2. This is because the 11 µm ATSR2-AIRS bias has a very small (slope = 0.00061) temperature dependent gradient which is even smaller in the 12 µm ATSR2-AIRS bias (beyond 40 RU, slope = ~ 0.00) although the 12 µm bias has a very small offset (−0.0030 RU). With ATSR-2 being a climate satellite, the slight slope in the 11 µm bias and the cold dip is most likely an AIRS artifact. Similar biases are observed in AIRS IASI comparisons (Table 2). This is consistent with AATSR–ATSR2 comparisons that show nearly constant difference between the two for the 11 and 12 µm channels (Smith, 2012).

By combining the ATSR2–AIRS difference with the AIRS–IASI difference reported by Wang et al. (2010 and 2011), the expected difference between the IASI and ATSR2 for the 11 and 12 µm channel can be estimated.

Finally the offset is calculated by combining the IASI-ATSR2 bias with the AATSR-IASI bias. For the 11 µm the offset is 0.0642 and 0.0935 $\mathrm{mW\,(m^2\,sr\,cm^{-1})^{-1}}$ for 12 µm and the true value is obtained by adding this offset to the IASI value.

$$\text{True Value (11 µm)} = X - Y(11\,\mu\text{m}) + 0.0642$$

$$\text{True Value (12 µm)} = X - Y(12\,\mu\text{m}) + 0.0935$$

Here X is the IASI radiance value and Y is the polynomial fit to the AATSR IASI difference. Its coefficients are listed in Table 3. This empirical procedure not only corrects for any calibration biases inherent in the AATSR (revealed in Pre-launch testing Fig. 3) but also corrects additional bias acquired post launch. For the 11 µm this empirical technique corrects the AATSR radiance to within ±0.0814 $\mathrm{mW\,(m^2\,sr\,cm^{-1})^{-1}}$ and at 12 µm

AMTD
8, 9785–9821, 2015

it corrects to within ±0.0623 mW $(m^2\,sr\,cm^{-1})^{-1}$y. Figure 10 shows the status of bias at each stage of the correction process for the 11 and 12 µm channel.

4 Conclusions

Using AATSR–IASI collocations that spanned 39 months (January 2008–March 2011) we have analyzed the trust-worthiness of AATSR and IASI measurements and their feasibility in being used as a reference for AVHRR re-calibration for the 11 and 12 µm IR channels.

This trustworthiness is measured by measuring scan angle, scene temperature and time dependence of the AATSR–IASI bias on a wide temperature range of 200–300 K for the 11 and 12 µm channels. Our inter-comparison shows that the nadir views of the AATSR and IASI are trustworthy and are good candidates for use in re-calibration of AVHRR.

In terms of scene temperature, the AATSR IASI inter-comparison bias curve is similar to the AATSR pre-launch curve (within a few hundredths of a K) in the 11 µm channel (Fig. 3) if an offset of 0.07 K (thought to be an IASI offset) is taken into account. In addition, for the same channel there is a very small dependence of bias with scan angle (Fig. 1). This has led to our conclusion that the dependence of the AVHRR IASI bias that was earlier documented by Blumstein et al. (2007), Wang and Cao (2008) and later by Mittaz and Harris. (2011) is primarily an AVHRR effect and not an IASI effect. The scan angle dependence of AATSR–IASI bias in the forward view (Fig. 1) may be due to geolocation errors in the AATSR forward view.

There are known issues with the AATSR 12 µm channel. We analyzed this problem and suggested a solution. Our analysis shows that this BT offset, which was earlier estimated to be of the order of −0.2 K (Corlett, 2014), actually varies with scene temperature and instrument temperature dependencies, and it can grow up to +0.4 K at low temperatures (∼ 210 K). Our attempts to remove this temperature dependent BT offset have revealed that shifting the SRF (in either direction) does not remove this bias. How-

AMTD
8, 9785–9821, 2015

ever, the bias is stable so we have developed an empirical technique to correct it. In this technique, the temperature dependence of this bias was first quantified by fitting a sixth degree polynomial and the final correct value of TOA measurement was taken as the corrected IASI radiance + offset. The offset was calculated by taking into account a comparison of IASI with a third instrument (namely the AIRS) and subsequent comparison of AIRS with an AATSR family instrument (namely the ATSR2). We applied this method to the to get empirical fits that correct the bias of the AATSR 11 and 12 µm channels to within $(\pm 0.0814\,\mathrm{mW\,(m^2\,sr\,cm^{-1})^{-1}}$ for 11 µm, $\pm 0.0623\,\mathrm{mW\,(m^2\,sr\,cm^{-1})^{-1}}$ for 12 µm). This analysis also suggests that the AIRS has a small wavelength dependent bias (Fig. 7).

Finally, Fig. 6 shows the temporal dependence of the AATSR–IASI bias for the 11 and 12 µm channels. This figure also shows that the 11 µm AATSR–IASI bias has a seasonal variation around the mean (of the order of 100th of a K) in the SST temperature range. However at low temperature (200–230 K) the winter months show slightly larger amplitude than the summer months. Compared to the 11 µm, the 12 µm channel shows a larger seasonal variation (0.042 ± 0.032 K) in the SST temperature range and 0.31 ± 0.03 K for the cold temperature range. For this channel, the bias in the cold temperature range seems to be directly influenced by instrument temperature (Fig. 6).

Figure 6 also shows temporary spikes in November–December of 2008/09. These are followed by year end orbital maneuvers (Noll, 2010). However in 2010/11 (DJF), Fig. 7, we see an enhanced spike (compared to previous years) at lower temperature ranges (i.e., < 230 K) in AATSR–IASI. Our analysis reveals that this trend is confined to collocations over Greenland and is most likely a caused by geo-location errors when orbital parameters (lowering of altitude and switch of orbit inclination control was done in October 2010) of ENVISAT were changed in order to prolong its life.

The main conclusion from the point of view of using AATSR as a reference is that the nadir view of the AATSR and AATSR measurements taken between latitudes 60° N–60° S give the most trustworthy measurements of the TOA radiances that can be used as a reference in re-calibration activities.

AMTD
8, 9785–9821, 2015

Acknowledgements. We wish to thank Bob Kuligowski from NOAA for his suggestions on improvement of this article.

References

Blumstein, D., Tournier, B., Cayla, F. R., Phupin, T., Fjortoft, R., Bull, C., and Ponce, G.: In flight performance of the Infrared Atmospheric Sounding Interferometer (IASI) on Metop-A, P. SPIE, 6684, 66840H, doi:10.1117/12.560907, 2007.

Cocevar, P.: ENVISAT – AATSR CYCLIC REPORT #98, ESA, 1–19, available at: https://earth.esa.int/sppa-reports/envisat/aatsr/cyclic/2010-12-26/AATSR_CR_98_101226_110125.pdf (last access: 14 September 2015), 2011.

Cocevar, P.: IDEAS – Envisat AATSR Performance Report, IDEAS-VEG-OQC-REP-1143, ESA, 1–46, https://earth.esa.int/documents/10174/437508/Envisat_AATSR_Performance_Report.pdf (last access: 14 September 2015), 2013.

Corlett, G.: AATSR SSES, 9th GHRSST-PP Science Team, Perros Guirec, 9–13 June 2008, 2008.

Corlett, G. K.: (A)ATSR Validation Activities, available at: http://atsrsensors.org/pdf/ATSRValidationIssues.pdf (last access: 14 September 2015), University of Leicester, UL-AATSR-VIR, 5B, 2014.

Clerbaux, C., Hadji-Lazaro, J., Turquety, S., George, M., Coheur, P. F., Hurtmans, D., Wespes, C., Herbin, H., Blumstein, D., Tourniers, B., and Phulpin, T.: The IASI/MetOp Mission: first observations and highlights of its potential contribution to GMES, Space Research Today, 168, 19–24, 2007.

EUMETSA T.: IASI Level 1 Product Guide, Ref: EUM/OPS-EPS/MAN/04/0032, Issue v3j, EUMETSAT, 1–110, available at: http://www.eumetsat.int/website/wcm/idc/idcplg?IdcService=GET_FILE&dDocName=pdf_iasi_level_1_prod_guide&RevisionSelectionMethod=LatestReleased&Rendition=Web (last access: 14 September 2015), 2012.

Illingworth, S. M., Remedios, J. J., and Parker, R. J.: Intercomparison of integrated IASI and AATSR calibrated radiances at 11 and 12 µm, Atmos. Chem. Phys., 9, 6677–6683, doi:10.5194/acp-9-6677-2009, 2009.

AMTD
8, 9785–9821, 2015

Leroy, S. S., Anderson, J. G., and Ohring, G.: Climate signal detection times and constraints on climate benchmark accuracy requirements, J. Climate, 21, 841–846, doi:10.1175/2007JCLI1946.1, 2008.

Llewellyn-Jones, D. Edwards, M. C., Mutlow, C. T., Birks, A. R., Barton, I. J., and Tait, H.: AATSR: global-change and surface-temperature measurements from Envisat, ESA Bull.-Eur. Space, 105, 11–21, 2001.

Mittaz, J. P. D. and Harris, A. R.: A physical method for the calibration of the AVHRR/3 thermal IR channels. Part II: An in-orbit comparison of the AVHRR long wave thermal IR channels on board MetOp-A with IAS, J. Atmos. Ocean. Tech., 28, 1072–1087, 2011.

Miranda, N. Duesmann, B., Pinol, M., Giudici, D., and D'Aria, D.: Impact of the Envisat Mission Extension on SAR data, available at: http://earth.esa.int/pub/ESA_DOC/ENVISAT/Impact_of_Envisat_Mission_Extension_on_SAR_data_-_1_01.pdf (last access: 12 September 2015), 2010.

Noll, C. E.: The Crustal Dynamics Data Information System, a resource to support scientific analysis using space geodesy, in: DORIS Special Issue: Scientific Applications in Geodesy and Geodynamics, edited by: Willis, P., Adv. Space Res., 45, 1421–1440, doi:10.1016/j.asr.2010.01.018, 2010.

Ohring, G., Wielicki, B., Spencer, R., Emery, B., and Datla, R.: Satellite instrument calibration for measuring global climate change – report of a Workshop, B. Am. Meteorol. Soc., 86, 1303–1313, 2005.

Phulpin, T., Prel, F., Blumstein, D., Tournier, B., Prunet, P., and Schlüssel, P.: Applications of IASI on MetOp-A: first results and illustration of potential use for meteorology, climate monitoring, and atmospheric chemistry, Optical Engineering + Applications, International Society for Optics and Photonics, 1–36, 2007.

Smith, D. L.: Effect of long wavelength response in AATSR filters on brightness temperature measurements, AATSR Technical Note, PO-TN-RAL-AT-0541, Issue 1.0, Rutherford Appleton Laboratory, 2007.

Smith, D. L.: Experience learned and recommendations from ENVISAT AATSR Calibration, Sentinel-3 calibration and Validation Planning Meeting, ESA/ESRIN, available at: http://congrexprojects.com/docs/12m17_docs/s3cvt\T1\textemdashsmith-d\T1\textemdashexperience-from-aatsr.pdf?sfvrsn=2 (last access: 12 September 2015), 2012.

Smith, D., Delderfield, J., Drummond, D., Edwards, T., Mutlow, C., Read, P., and Toplis, G.: Calibration of the AATSR instrument, Adv. Space Res., 28, 31–39, 2001.

AMTD
8, 9785–9821, 2015

Smith, D., Mutlow, C., Delderfield, J., Watkins, B., and Mason, G.: ATSR infrared radiometric calibration and in-orbit performance, Remote Sens. Environ., 116, 4–16, 2012.

Snel, R.: In-orbit optical path degradation: gome experience and sciamachy prediction, in: Proceedings of the ERS-ENVISAT Symposium, ESA Publications Division, Nordwijk, the Netherlands, SP-461 (on CD ROM), 16–20 October 2000, Gothenburg, Sweden, 2001.

Tanzi, C. P.: Degradation of UV earth albedo observations by Global Ozone Monitoring Experiment (GOME), in: Proceedings of the ERS-ENVISAT Symposium, ESA Publications Division, Nordwijk, the Netherlands, SP-461 (on CD ROM), 16–20 October 2000, Gothenburg, Sweden, 2001.

Wang, L. and Cao, C.: On-orbit calibration assessment of AVHRR longwave channels on MetOp-A using IASI, IEEE T. Geosci. Remote, 46, 4005–4013, doi:10.1109/TGRS.2008.2001062, 2008.

Wang, L., Wu, X., Goldberg, M., Cao, C., Li, Y., and Sohn, S.-H.: Comparison of AIRS and IASI radiances using GOES imagers as transfer radiometers toward climate data records, J. Appl. Meteorol. Climatol., 49, 478–492, doi:10.1175/2009JAMC2218.1, 2010.

Wang, L., Goldberg, M., Wu, X., Cao, C., Iacovazzi Jr., R. A., Yu, F., and Li, Y.: Consistency assessment of Atmospheric Infrared Sounder and Infrared Atmospheric Sounding Interferometer radiances: double differences versus simultaneous nadir overpasses, J. Geophys. Res., 116, D11111, doi:10.1029/2010JD014988, 2011.

Wu, D. L.: Mesoscale gravity wave variances from AMSU-A radiances, Geophys. Res. Lett., 31, L12114, doi:10.1029/2004GL019562, 2004.

Wu, X., Hewison, T., and Tahara, Y.: GSICS GEO-LEO inter-calibration: Baseline algorithm and early results, Proc. SPIE, 7456, 745604-1–745604-12, 2009.

Yu, F. and Wu, X.: Radiometric Calibration Accuracy of GOES Sounder Infrared Channels, IEEE T. Geosci. Remote, P-1187–1199, 51, doi:10.1109/TGRS.2012.2219625, 2012.

AMTD
8, 9785–9821, 2015

Table 1. Thresholds applied on collocated AATSR pixels in a single IASI pixel.

Thresholds	
SD Collocated Pixels	< 0.5 K
SD Perimeter	< 1 K
Time Difference	< 15 Mins
Time Span	Jan 2008–Mar 2011
Percentage of area of IASI pixel collocated with AATSR pixels	70 %
Sat Zenith Angle difference	1°

AMTD
8, 9785–9821, 2015

Table 2. IASI–AIRS radiance bias computed by Want et al. (2010, 2011) first by the direct SNO method and second using GOES-11 as transfer. RU is Radiance Units, $mW\,(m^2\,sr\,cm^{-1})^{-1}$.

Channel	IASI–AIRS 210–230 K (using SNO)	IASI–AIRS 295 K (using GOES-11 transfer)
11 µm	−0.0790 (±0.060) RU	−0.0433 (±0.016) RU
12 µm	−0.1471 (±0.062) RU	−0.0460 (±0.018) RU

AMTD
8, 9785–9821, 2015

Table 3. Coefficients of the polynomial fit to AATSR–IASI in radiance space.

	11 µm	12 µm
C0	−0.0893740	−0.134521
C1	−0.00762876	0.0210454
C2	0.000822220	−0.000512018
C3	-2.67709×10^{-5}	2.50340×10^{-6}
C4	4.05375×10^{-7}	4.15293×10^{-8}
C5	-2.97869×10^{-9}	-5.80190×10^{-10}
C6	8.62472×10^{-12}	2.09040×10^{-12}

AMTD
8, 9785–9821, 2015

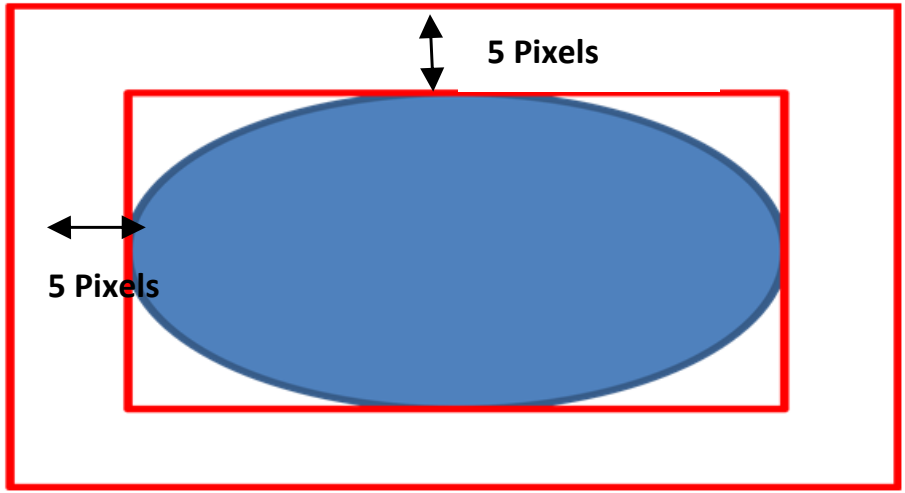

Figure 1. IASI foot print (blue) at nadir. The outer red boundaries indicate the perimeter area where the perimeter threshold is applied. This area is 5 AATSR pixels (5 km) wide. The Mean radiance of AATSR pixel collocated within the blue is compared with the IASI representative pixel radiance.

AMTD
8, 9785–9821, 2015

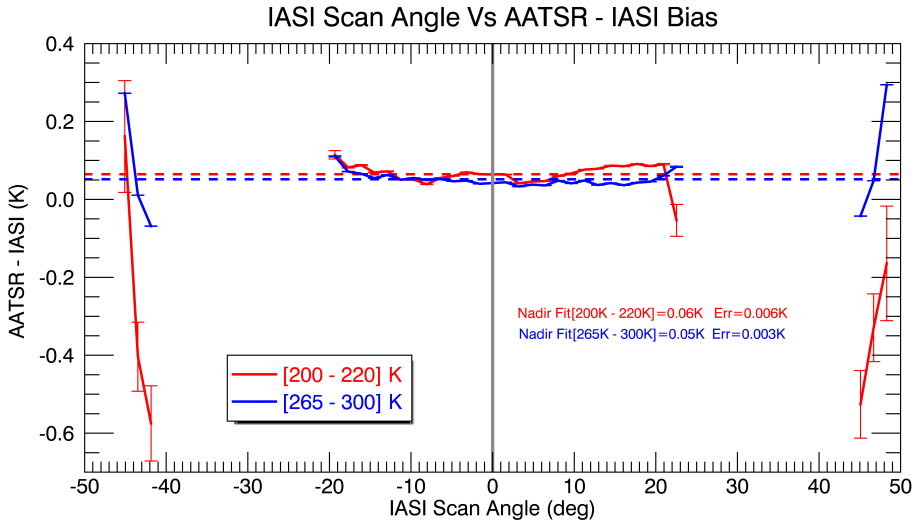

Figure 2. Scan angle dependence of the AATSR–IASI bias for cold (200–220 K) and SST (265–300 K) temperature ranges. Neither AATSR nor IASI show any scan angle dependence in the −20 to +20° scan angle range.

AMTD
8, 9785–9821, 2015

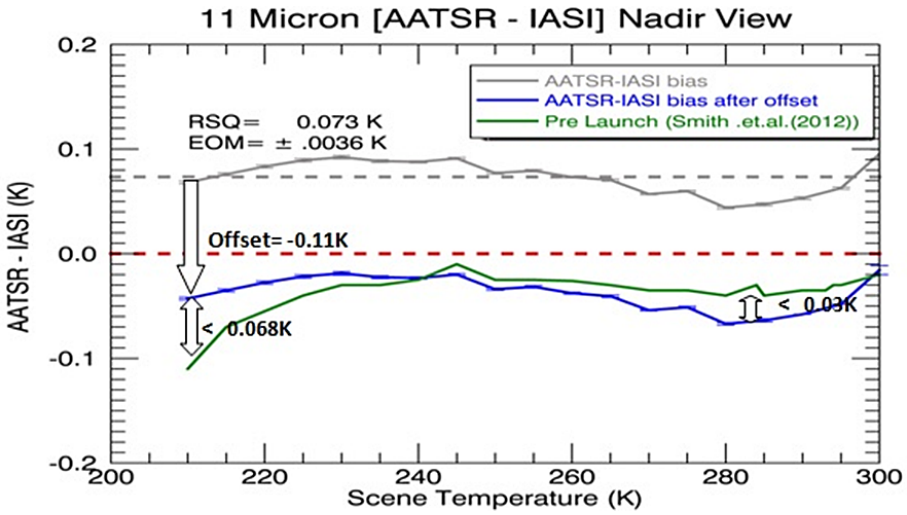

Figure 3. Similarity of the temperature difference between AATSR–IASI minus an offset of 0.11 K (i.e. post launch) and pre-launch (Smith et al., 2012). The grey curve shows the temperature dependence.

AMTD
8, 9785–9821, 2015

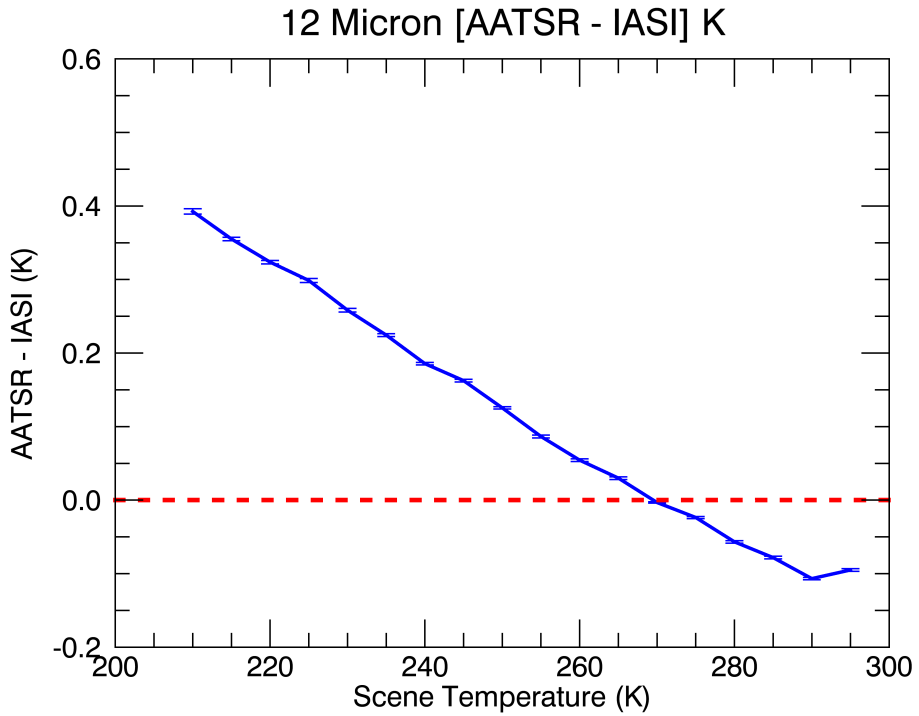

Figure 4. Temperature dependent bias of the AATSR–IASI for the 12 µm channel.

AMTD
8, 9785–9821, 2015

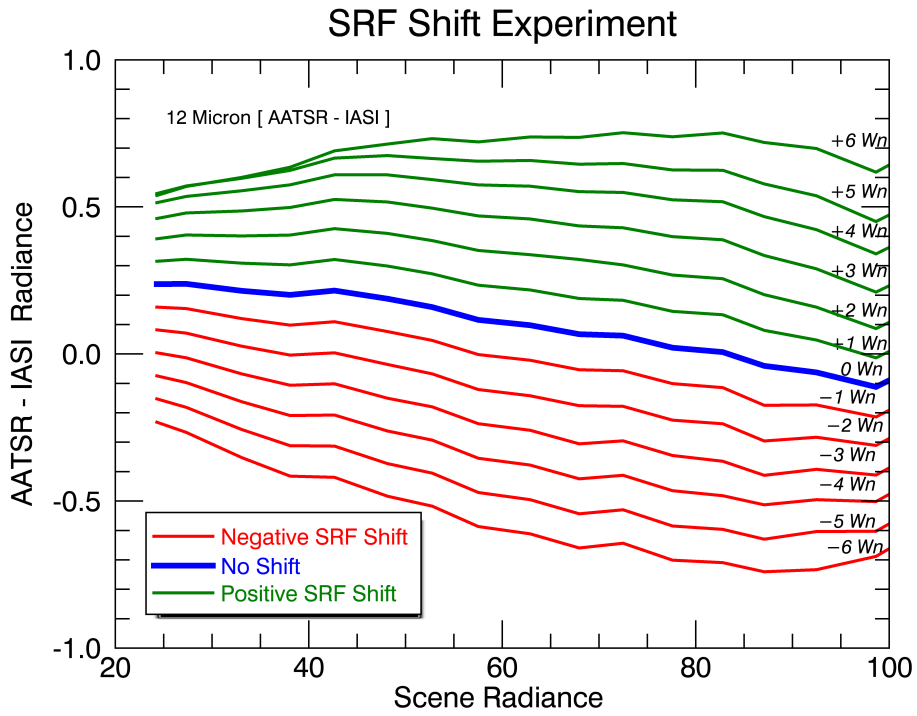

Figure 5. Impact of shifting the AATSR Spectral Response Function by six wave numbers on either side of its central Wn position in steps of 1 Wn. The scene temperature dependent nature of AATSR–IASI bias does not diminish by shifting SRF. Unit of scene radiance is mW $(m^2\,sr\,cm^{-1})^{-1}$.

AMTD
8, 9785–9821, 2015

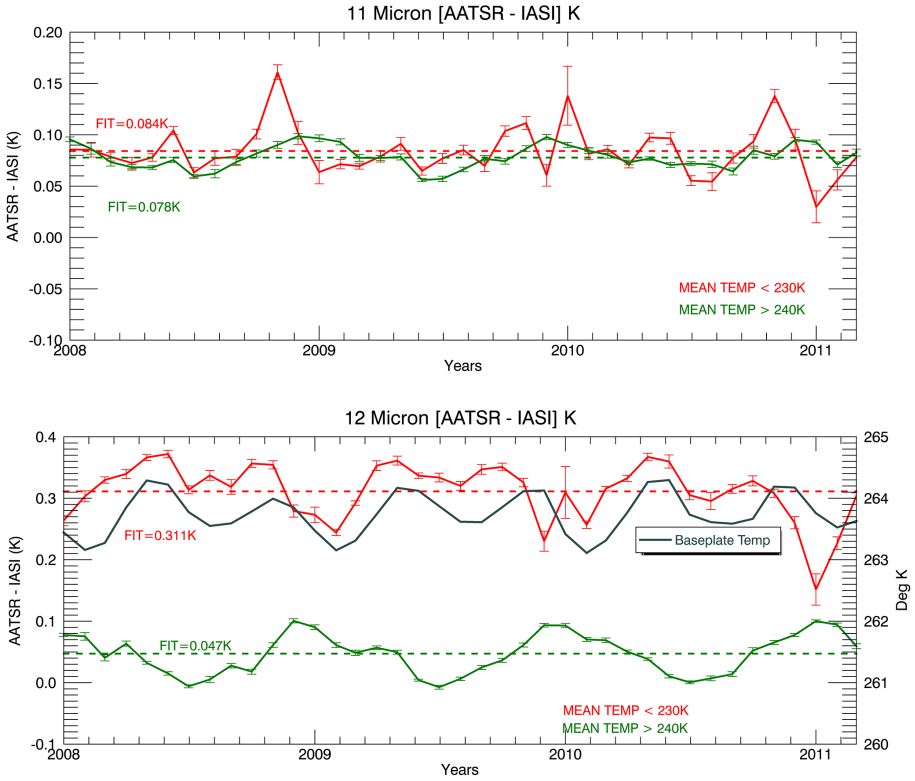

Figure 6. Time series of variation of AATSR IASI bias for 11 and 12 µm channels. in the cold (red) and warm temperature (green) ranges. The bias at cold temperature in 12 µm is highly correlated with the instrument temperature.

AMTD
8, 9785–9821, 2015

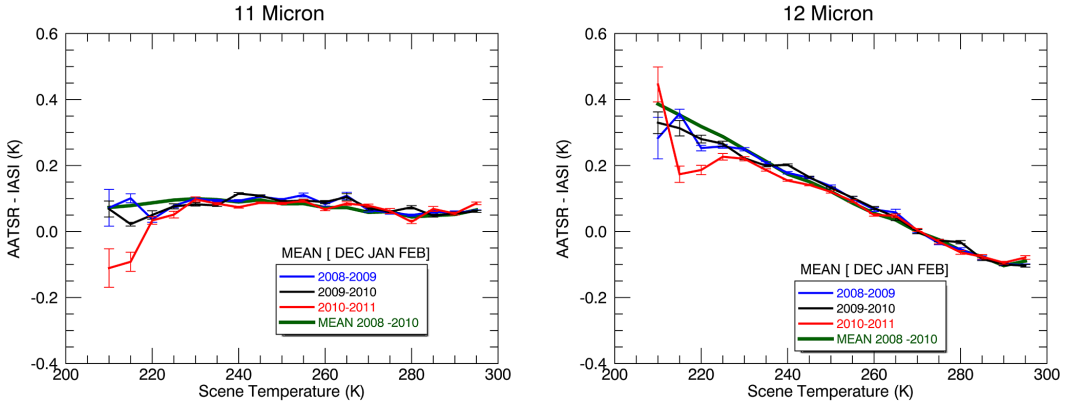

Figure 7. Year to year AATSR IASI bias for DJF for the 11 and 12 µm channels. An anomalous trend at cold temperature is clearly visible in 2010/11 DJF.

AMTD
8, 9785–9821, 2015

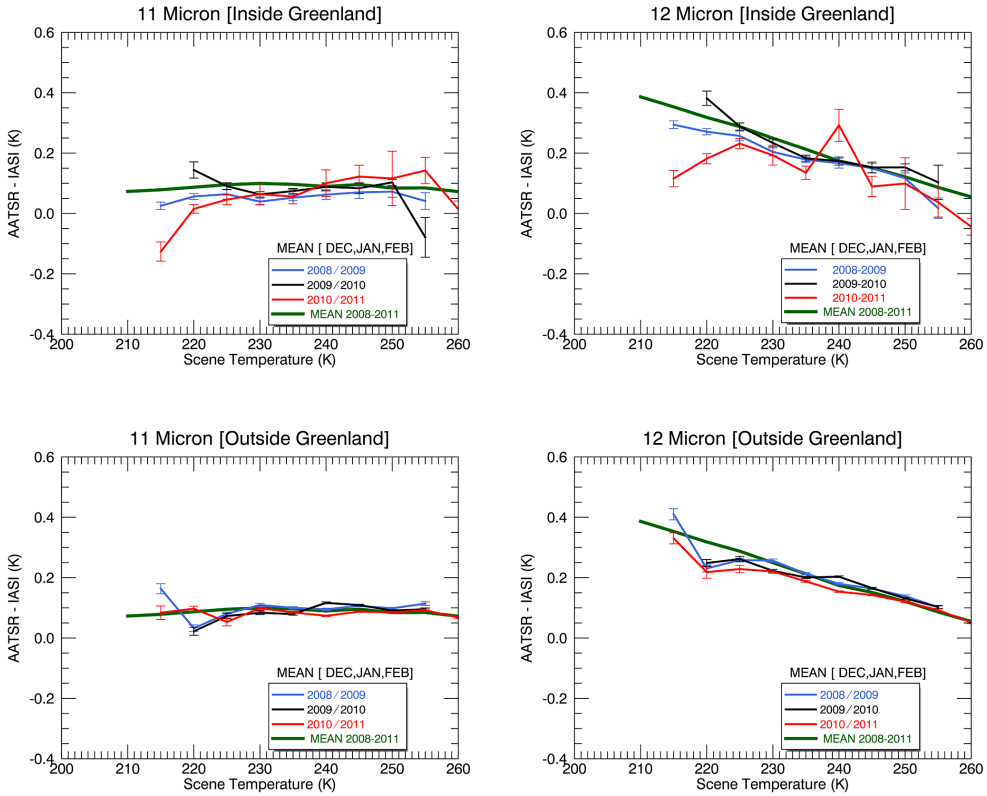

Figure 8. Comparison of AASR–IASI bias over Greenland and outside Greenland. The anomalous trend seen in 2010/11 DFJ AATSR–IASI bias is mainly confined to Greenland.

AMTD
8, 9785–9821, 2015

Inter-comparison of IASI and AATSR over an extended period

M. Bali et al.

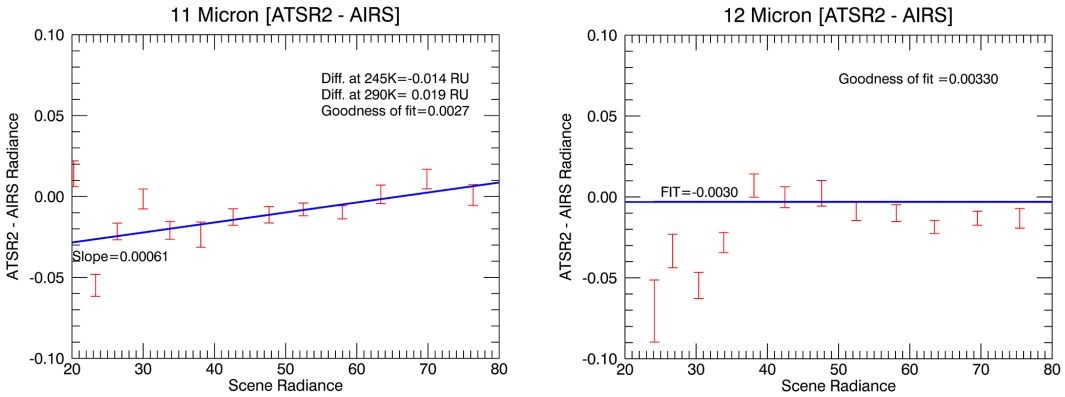

Figure 9. ATSR2–AIRS bias variation w.r.t radiance in $\mathrm{mW\,(m^2\,sr\,cm^{-1})^{-1}}$ for the 11 (L) and 12 (R) µm channel. RU is Scene Radiance and its units are $\mathrm{mW\,(m^2\,sr\,cm^{-1})^{-1}}$.

AMTD
8, 9785–9821, 2015

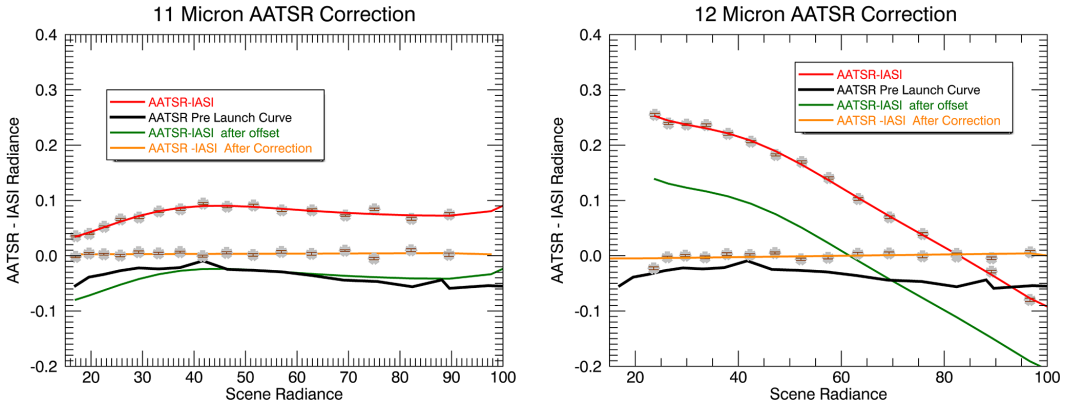

Figure 10. Output of each of the three steps of correcting the bias for the 11 and 12 µm channel. The red curve is the AATSR IASI difference in radiance space. The orange is the final value of AATSR value after applying the polynomial correction. All radiance units are in $\mathrm{mW\,(m^2\,sr\,cm^{-1})^{-1}}$.

AMTD
8, 9785–9821, 2015

Inter-comparison of IASI and AATSR over an extended period

M. Bali et al.